

International Conference on Space Optics—ICSO 2018

Chania, Greece

9–12 October 2018

Edited by Zoran Sodnik, Nikos Karafolas, and Bruno Cugny



Diode-pumped Alexandrite laser instrument for next generation satellite-based Earth observation

Michael Strotkamp

Alexander Munk

Bernd Jungbluth

Hans-Dieter Hoffmann

et al.



icso proceedings



DIODE-PUMPED ALEXANDRITE LASER INSTRUMENT FOR NEXT GENERATION SATELLITE-BASED EARTH OBSERVATION

Michael Strotkamp*^a, Alexander Munk^a, Bernd Jungbluth^a, Hans-Dieter Hoffmann^a, Josef Höffner^b
^aFraunhofer Institute for Laser Technology, Steinbachstr. 15, 52074 Aachen, Germany;
^bLeibniz Institute of Atmospheric Physics, Schlossstraße 6, 18225 Kühlungsborn, Germany

ABSTRACT

In this work the first diode-pumped Alexandrite ring laser in Q-switched single-longitudinal mode (SLM) operation is presented. A carefully designed and complex ring resonator with several functional components is combined with an innovative pumping scheme with high-power red laser diodes.

The spectral and energetic suitability of a first laser was demonstrated in hundreds of operating hours and, with a novel mobile lidar system, by the first measurements in the atmosphere by means of a diode-pumped Alexandrite laser, yielding data from the stratosphere to the mesosphere.

An improved laser yields a pulse energy of 1.7 mJ at a repetition rate of 500 Hz with an excellent beam quality of $M^2 < 1.1$. By seeding the resonator with a narrow-band diode laser, SLM operation with a linewidth below 4 MHz is achieved. The electro-optical efficiency of 2 % is the highest archived for all Alexandrite lasers in SLM operation and reasonable for space-operation.

The performance analysis as well as benchmarking with the space-qualified mounting technology point out the TRL and the remaining effort of development of the technology.

Keywords: Alexandrite laser, diode-pumped laser, ring laser, single-longitudinal mode laser, Q-switched laser, tunable laser, spaceborne laser, lidar

1. INTRODUCTION

Understanding temperature distributions and wind fields in the atmosphere at altitudes between 80 and 110 km, i.e. the mesosphere and lower thermosphere (MLT), is crucial for performing numerical simulations of the Earth's climate. The effects of gravity waves on the global wind system and atmospheric dynamics are hardly understood and item of research of space agencies and ground-based observations [1-6]. One well-established approach to provide such data is to measure the Doppler-broadened and -shifted resonance line of metal atoms, e.g. potassium (770 nm or 772 nm) [6, 7], iron (386 nm) [8, 9] and sodium (589 nm) [10-12], by means of a Doppler lidar.

While localized measurements have been performed over the last 20 years from the ground and revealed fundamental deviations from the predicted conditions, there is no coverage of global scale by lidar. The development of a spaceborne resonance lidar instrument is deferred by the lack of laser sources at the demanded wavelengths that are suitable for spaceborne operation.

The currently used Alexandrite ($\text{Cr}^{3+}:\text{BeAl}_2\text{O}_4$) lasers with their broad tunability (700-800 nm) [13] are well suited for the generation of several interesting wavelengths, either operating at their fundamental wavelength or intra-cavity frequency-doubled. The flashlamp-pumped Alexandrite ring lasers operating in Q-switched single-longitudinal mode (SLM) operation are commonly used as beam sources in resonance potassium and iron resonance lidar systems [6-9].

However the usage of flashlamps as pump source makes them unsuitable for spaceborne operation, due to the poor efficiency and limited lifetime. One hopeful approach to overcome these drawbacks is by replacing the flashlamps with diode lasers [14, 15]. Recently, new basic investigations in the field of diode-pumped Alexandrite lasers have been conducted with focus on altimetry lidar and vegetation monitoring (red-edge) [16] and resonance lidar [17].

*michael.strotkamp@ilt.fraunhofer.de; phone +49 241 8906-132; www.ilt.fraunhofer.de

Another approach to address a resonance line of iron with a lidar system is the usage of a Nd:YAG laser operating at 372 nm (third harmonic of 1116 nm) [9]. The advantage is the usage of well matured technology for Nd:YAG lasers but at the expense of a two-step nonlinear process.

To address the resonance line of sodium a 589 nm there are two approaches already aiming for a spaceborne mission by allowing leverage from previous space-qualified lasers. The first system uses the second harmonic of a Raman-shifted Nd:YVO₄ laser [11] and the second system is mixing the output of two Nd:YAG lasers, one emitting at 1064 nm and one at 1319 nm [12].

2. REQUIREMENTS

The requirements to the laser source can be derived from the application in a resonance lidar. Especially the spectral requirements are challenging because the metal resonance line is scanned to calculate its width and shift. This requires a linewidth of the laser below 30 MHz and consequently a laser with SLM operation.

The energetic requirements strongly depend on the specific metal line and the targeted resolution of the measurement but average power on the Watt level with pulse energies on the Millijoule level seem reasonable.

For a proof-of-principle a diode-pumped Alexandrite laser for a ground-based lidar measurement of potassium in the upper atmosphere (MLT ~80-100 km) is designed, that has the same spectral but slightly eased energetic requirements shown in Table 1. A spaceborne laser can, if necessary, be scaled in energy by means of a subsequent amplifier stage without altering its spectral or temporal parameters.

Table 1: Requirements on a laser source for potassium resonance lidar measurements in the upper atmosphere

Parameter	Requirement
Pulse energy	> 1 mJ
Repetition rate	> 150 Hz
Electro-optical efficiency	> 1 %
Pulse duration	50 – 1000 ns
Wavelength	769.898 nm (potassium resonance line in air)
Linewidth	~99% < 30 MHz, single-mode (lorentz)
Frequency shift	< 50 MHz
Frequency jitter	< 10 MHz
Beam quality	$M^2 < 1.5$
Pointing stability	< 10 μ rad

The lasers we present here are Alexandrite lasers with a ring resonator pumped by two laser diode modules. The ring resonator ensures a travelling wave to prevent spatial hole burning and its resonator length is stabilized to match it to a narrow-band diode laser. It also comprises a Faraday rotator for unidirectional operation and a Pockels cell for Q-switching to ensure suitable pulse durations. The two laser diode modules provide the sufficient pump energy and a high electro-optical efficiency. The energetic and spatial properties of the laser diode modules have high impact on the resonator design because of the thermal lens induced by the pump energy deployed in the crystal.

2.1 Specification of the pump modules

The pump modules used for the Alexandrite lasers are commercially available diode lasers emitting in the red spectral range. Within each module the beams from seven diode bars are collimated and optically combined to provide 100 W of pulse peak power, as shown in Figure 1 (a), with an electro-optical efficiency of 33 %. The output wavelength changes slightly (< 0.2 nm/°C) with the temperature, influenced by cooling-water temperature, pump current and duty cycle, and

is about 636 nm at the working point, see the inset in Figure 1 (a). The module provides an output beam with an unbalanced beam quality of about $M^2 = 30$ in fast-axis and $M^2 = 300$ in slow-axis. The beam quality and the peak power are unaffected by the repetition rate (from 100 Hz to 500Hz) or the pump pulse duration up to a duty cycle of 5 %.

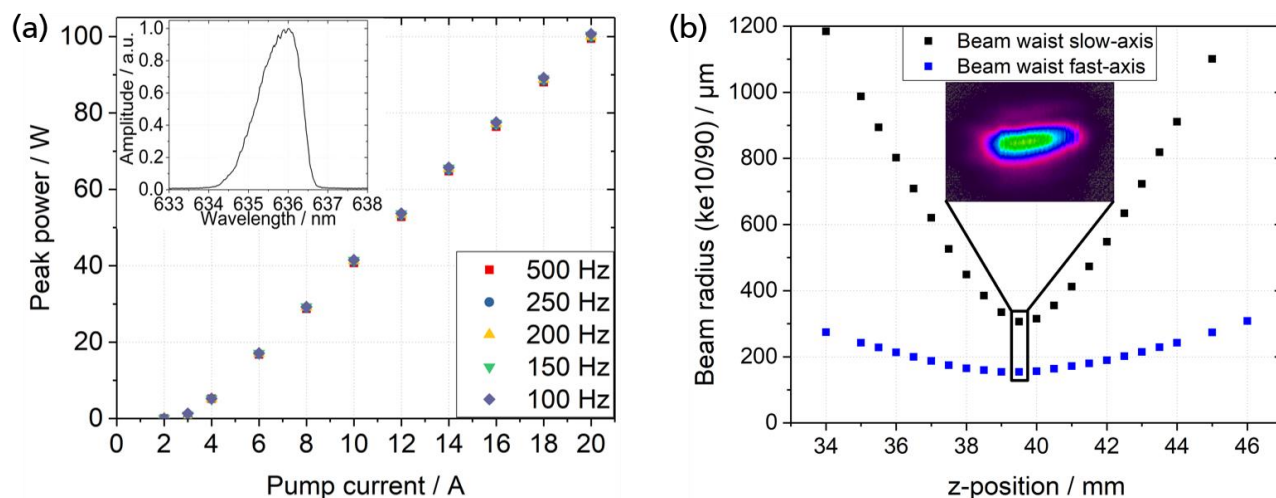


Figure 1. (a) Pulse peak power as a function of the pump current for different repetition rates and spectrum of the diode pump module at 20 A pump current, 200 μs pulse length and a repetition rate of 250 Hz (inlet). (b) Beam caustic in fast-axis and slow-axis behind pump optics and beam profile in the focus (inlet).

3. DEMONSTRATOR

3.1 Pump optics design

In a first setup one diode module is used to longitudinally pump one Alexandrite crystal each. The linear polarized light is absorbed in a single-pass through the crystal. With a combination of five cylindrical and spherical lenses the output beam of each diode module is shaped to generate pump spots with waist radii of 150 μm in fast-axis and 300 μm in slow-axis inside the Alexandrite crystals. The corresponding caustic is plotted in Figure 1 (b). The total length of the beam shaping from the diode pump module to the crystal is 215 mm. The optics design and opto-mechanical setup is based on off-the-shelf components and has not yet been optimized for simplicity or compactness.

3.2 Laser design

The Alexandrite crystal is longitudinally pumped so that the spatial overlap of the pumped volume of the crystal with the laser mode and, therefore, the laser efficiency is maximized. However, due to the low beam quality and large divergence of the pump beam in the slow-axis, the pumping mirror is placed directly in front of the laser medium for the pump light to pass through the aperture without diffraction or even clipping. Since there is such a short distance between the mirror and the crystal's facet, the beam path of the laser mode has to be redirected through the laser medium after its reflection. The incoming and outgoing beams are separated by a small angle and split by means of a scraper mirror to form a ring cavity. This geometry also increases the spatial overlap between the laser mode and the highly divergent pump mode in slow-axis and, consequently, the laser gain and prevents lasing in higher transversal mode operation.

To reach the necessary pulse energy, two Alexandrite crystals, each pumped by one laser module, are used for the ring laser. The Alexandrite crystals used as laser media have an aperture of 4*4 mm² and a length of 7 mm with a Cr³⁺-doping-concentration of 0.2 at%, absorbing more than 95 % of the incident pump light. For optimized laser performance at the required output wavelength, the Alexandrite crystals are operated at elevated temperatures. In our setup, the best laser performance for an output wavelength of 770 nm is observed at 115 °C.

The setup of the resonator is shown in Figure 2. It comprises, aside from the two crystals, two dichroic pumping mirrors with high transmission for the pump wavelength, several highly reflective mirrors for the laser wavelength, a Brewster-

angled Pockels cell and a thin-film polarizer (TFP) to allow Q-switching, a half-wave plate for polarization adjustment, a Faraday rotator for unidirectional operation and a plane output coupler with 3 % transmission for the laser wavelength. One of the plane mirrors is mounted in a mirror mount with piezo-driven adjusters so that the resonator can be adjusted remotely. To compensate for the stronger thermal lens in fast-axis, one of the pumping mirrors is a highly reflective convex cylindrical mirror with a radius of curvature of +200 mm in the direction of the fast-axis. The spherical concave mirrors have radii of curvature of -1000 mm and -750 mm, respectively. The total length of the resonator is approximately 1000 mm.

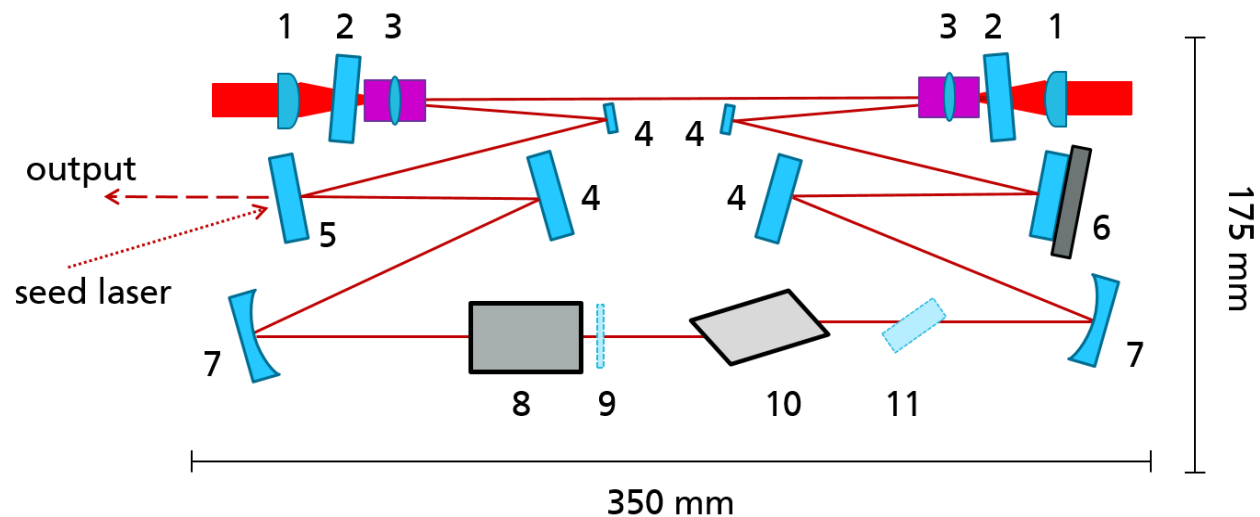


Figure 2. Schematic setup of the ring cavity with numbered cavity elements: Focusing lens (1), pumping mirror (2), Alexandrite crystal with intrinsic thermal lens (3), flat folding mirrors (4), output coupler (5), mirror on piezo-actor for stabilization of the cavity length (6), convex curved mirror (7), Faraday Rotator (8), half-wave plate (9), Brewster Pockels cell (10), thin-film polarizer (11).

SLM operation of the Alexandrite laser is achieved by a commercial external cavity diode seed laser that operates at the desired wavelength in cw operation. The linewidth of the seed laser is < 1 MHz and the output power is about 20 mW. To achieve SLM operation, the seed laser is spatially matched with the resonator mode and the cavity length is matched to the desired wavelength. The cavity length is adjusted by one of the plane resonator mirrors mounted on a piezo actuator ((6) in Figure 2). Stabilized SLM operation can be achieved using the ramp-and-fire method described in [18].

3.3 Experimental results

The following experimental results are achieved in SLM operation with a pump pulse duration of 170 μ s, a pump current of 20 A and a repetition rate of 150 Hz. The laser yields, as shown in Figure 3 (a), a pulse energy of 1.1 mJ with a stability of 5 % relative standard deviation. The demonstrated stability complies with the requirements for a lidar measurement since the calculation is calibrated on the measurement of the energy of each pulse.

The laser beam has a Gaussian beam profile, as shown in Figure 3 (b), and a beam quality of $M^2 < 1.2$ in both direction. Due to the cylindrical optics and the significantly different thermal lens, the output beam is elliptical and astigmatic. But beam shaping by means of cylindrical lenses results in a round beam profile and a stigmatic laser. The Faraday rotator inside the resonator ensures reliable unidirectional operation and the polarization of the emitted light is 100 % linear.

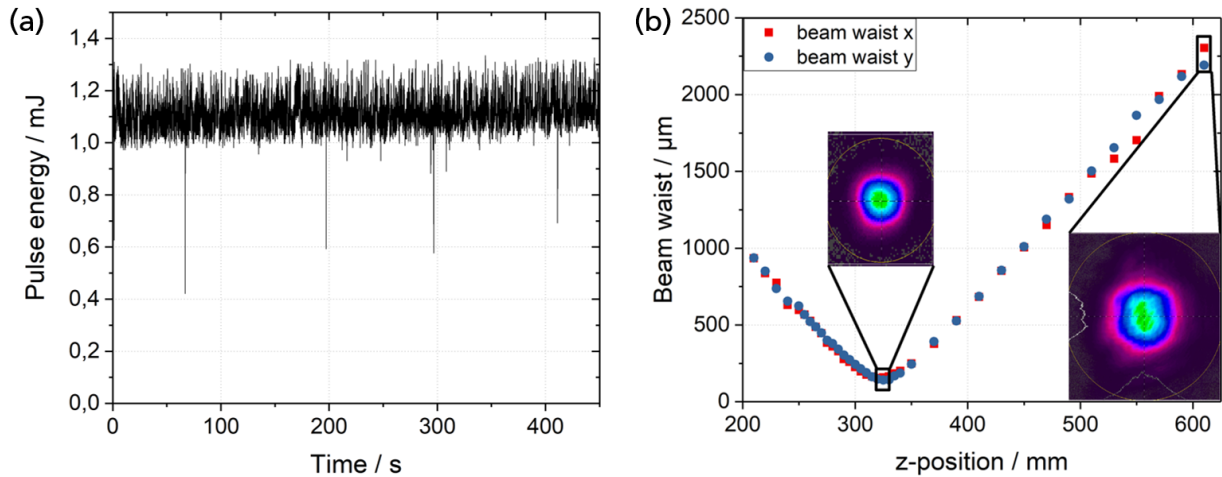


Figure 3. (a) Pulse energy in SLM operation over time. (b) Caustic of the laser in single-longitudinal mode operation after cylindrical beam shaping with beam profiles in focus and far field

The output wavelength of the unseeded oscillator is 769 nm with a broadband substructure over 1.5 nm. Seeding the cavity and stabilizing the cavity length with the use of the ramp-and-fire method decreases the linewidth significantly, resulting in a linewidth below the spectral resolution of the spectrometer (4 pm or 2 GHz), shown in Figure 4 (a). Laboratory measurements of the linewidth of the laser after integration in a novel lidar system indicate a linewidth of approximately 10 MHz. Figure 4 (b) shows the temporal shape of the pulse which has a pulse width of 420 ns with the pulse build-up time being approximately 5 μs .

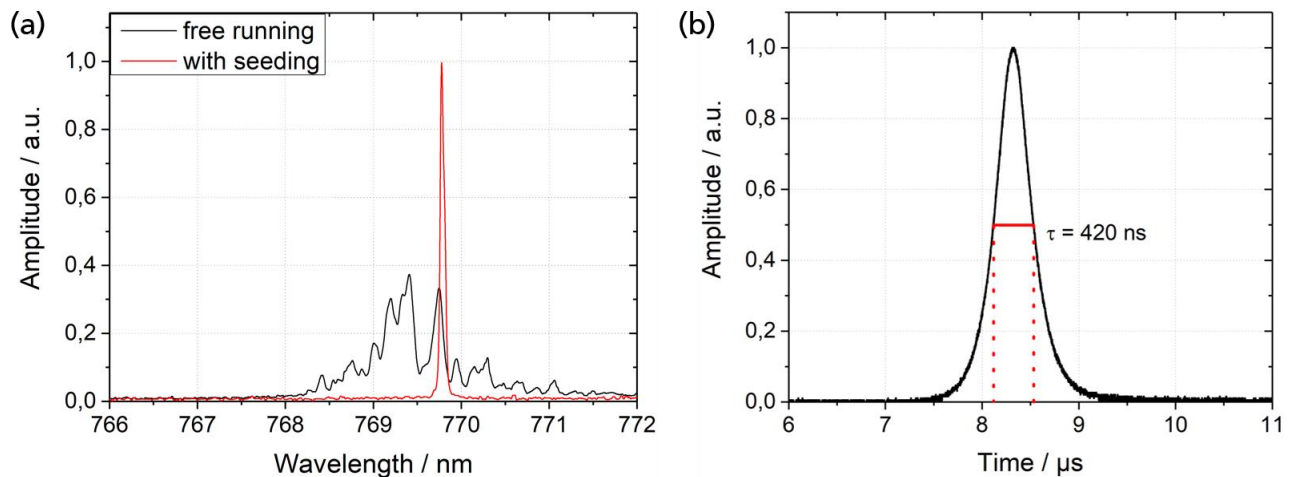


Figure 4. (a) Optical spectrum of the Q-switched ring laser with and without seeding. (b) Pulse shape in single-longitudinal mode operation.

Additionally, the repetition rate can be scaled up to 320 Hz without any change of the resonator optics. At this repetition rate the pump pulse duration is reduced to 135 μs , corresponding to a total pump pulse energy of 26 mJ. This results in a slightly lower pulse energy of 0.65 mJ and longer pulse durations of 800 ns while SLM operation and the spatial beam profile is sustained. With these parameters, below 4 MHz linewidth has been achieved.

Figure 5 shows the first atmospheric measurements conducted within a mobile lidar system at the Leibniz IAP in Kühlungsborn, proving the suitability of the laser. Despite the tentative setup of the receiver of the lidar system, the detected light indicates the potassium layer at a height of 80 to 100 km. Detailed information on these measurements and

the lidar system are presented in another presentation at this conference and will be published in more detail soon. Up to now the spectral and energetic suitability of the laser was demonstrated in hundreds of operating hours.

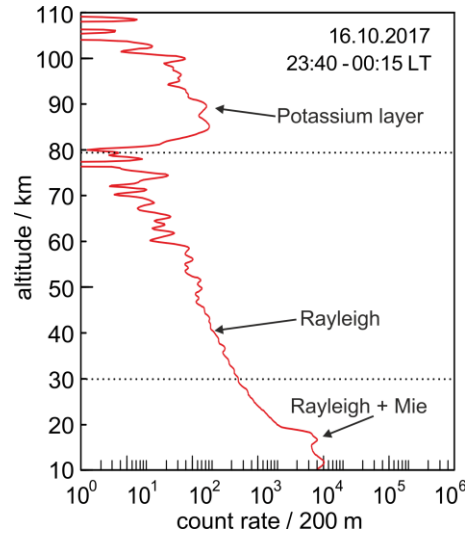


Figure 5. First atmospheric measurements of the potassium layer with the diode-pumped alexandrite laser.

4. IMPROVED DEMONSTRATOR

The first laser demonstrated with the lidar measurement the proof-of-principle that a diode-pumped Alexandrite laser can meet the high spectral requirements of a resonance lidar. The complex resonator design is a result from the spatial properties of the pump modules, e.g. the unbalanced beam quality in fast- and slow-axis, and shows high dependence of the laser mode properties to changes of the thermal lenses in the Alexandrite crystals. The alignment of the resonator is difficult due to the acentric double-pass of the laser mode through the pumped crystal and thereby the thermal lens.

4.1 Pump optics design

To overcome these drawbacks, the two pump modules are polarization-coupled and symmetrized by means of step mirrors [19] to balance the beam qualities and provide a round pump beam cross section. After the pump optics, the beam quality is $M^2 = 100$ in fast- and $M^2 = 150$ in slow-axis. The focus radii in the crystal are $w = 150 \mu\text{m}$ in fast- and $w = 210 \mu\text{m}$ in slow-axis. An extract of the measured caustic around the focus is plotted in Figure 6. The combined pulse energy behind all pump optics is 24 mJ with a pump pulse duration of 120 μs .

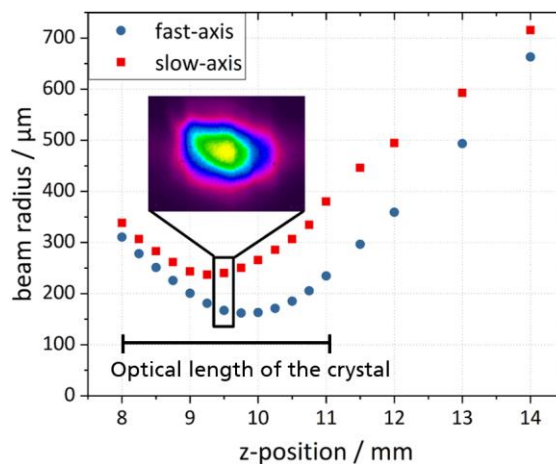


Figure 6. Beam radius of the pump light over the crystal length with beam profile at the focus position (inlet). The resulting effective beam radius inside the crystal is 205 μm in fast- and 257 μm in slow-axis.

Because the absorption of pump light is a magnitude lower for light at 636 nm vertically polarized to the b-axis of the crystal [13], 40 % of the polarization-coupled pump light is not absorbed at its single pass through the laser crystal, which has a dopant concentration of 0.29 at%. The transmitted pump light is collimated behind a second pumping mirror, reduced in its size by a telescope, its polarization adjusted by a quarter-wave plate and refocused into the crystal. The backfolded light is absorbed on its way back through the crystal and guarantees a homogeneously pumped crystal.

4.2 Laser design

The laser resonator is schematically shown in Figure 7. It comprises, compared to the first laser design, only one Alexandrite crystal with an aperture of $2 \times 2 \text{ mm}^2$ and a length of 7 mm that is operated at a temperature of $105 \text{ }^\circ\text{C}$. It has a total length of approximately 2000 mm and consists of the same components as the first laser but the two concave mirrors have a radius of curvature of -900 mm and both pumping mirrors are plane. The output coupler also has a reflectance of $R = 0.97$ for the laser wavelength

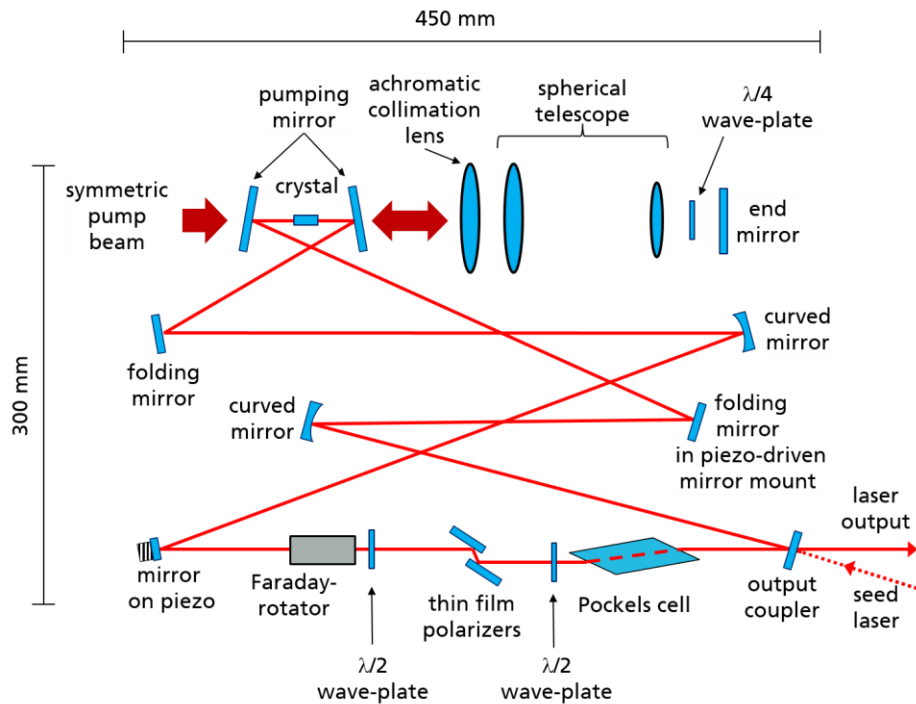


Figure 7. Schematic drawing of the resonator including the backfolding of the transmitted pump light.

The resonator is designed for a laser beam radius of around $200 \text{ }\mu\text{m}$ in the crystal which results in a good overlap with the pump beam. The beam radius on the critical optical components like the Pockels cell or the Faraday rotator is around $700 \text{ }\mu\text{m}$, preventing laser induced damage.

4.3 Experimental results

In Q-switched operation the laser yields a pulse energy of 1.7 mJ and features a high pulse-to-pulse stability of 0.2% at a repetition rate of 500 Hz , resulting in an average power of 0.85 W with a pulse duration of 850 ns . A measurement of the pulse energy over time is plotted in Figure 8 (a). Taking into account the electro-optical efficiency of the diode modules of 33% and the transmission losses of the pump optics of approximately 20% , the laser features an electro-optical efficiency of 2% .

The output beam is round and stigmatic so that no additional cylindrical beam shaping is necessary. The beam profile of the laser has a Gaussian shape with a beam quality of $M^2 \leq 1.1$ in both spatial directions. A caustic of the output beam with beam profiles at selected positions of the optical axes is plotted in Figure 8 (b).

The linewidth of the seeded and stabilized laser remains below 10 MHz .

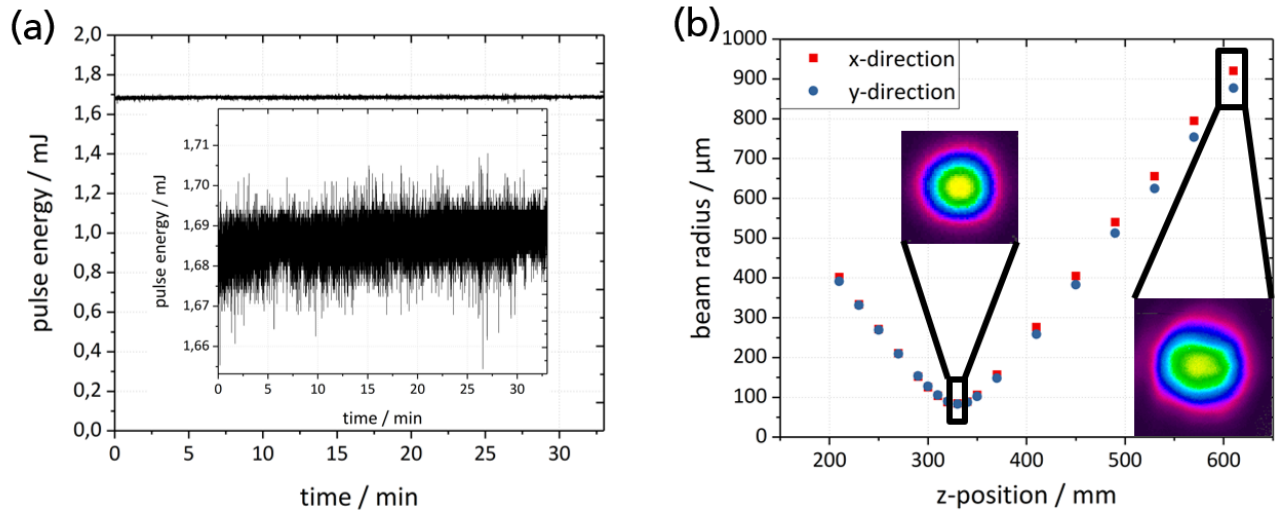


Figure 8. (a) Measured pulse energy in Q-switched operation over more than 30 minutes with a zoom on the relevant energy regime as inset and (b) Beam radius of output beam plotted against propagation length with inset of intensity profile at designated positions. The resulting beam qualities are $M^2 = 1.09$ in x-direction and $M^2 = 1.06$ in y-direction

The laser's average power is more than five times higher with a pulse energy stability one magnitude higher and the electro-optical efficiency is doubled compared to the first demonstrator. Additionally due to the symmetric pump beam and careful laser design the laser is easier to align and less sensitive against changes of the thermal lens or misalignment compared to its predecessor. The requirements set by the application are fulfilled as shown in Table 2.

Table 2: Requirements and achieved parameters

Parameter	Requirement	Achieved
Pulse energy	> 1 mJ	1.7 mJ
Repetition rate	> 150 Hz	500 Hz
Electro-optical efficiency	> 1 %	2 %
Pulse duration	50 – 1000 ns	400 – 850 ns
Wavelength	769.898 nm (potassium resonance line in air)	769.898 nm
Linewidth	< 30 MHz (~99%), single-mode (lorentz)	< 4 MHz
Frequency shift	< 50 MHz	< 10 MHz
Frequency jitter	< 10 MHz	< 1 MHz
Beam quality	$M^2 < 1.5$	$M^2 < 1.1$
Pointing stability	< 10 μ rad	< 3 μ rad

5. SUITABILITY FOR SPACEBORNE APPLICATION

For the evaluation of the laser design regarding stability under space condition, a performance analysis is carried out. The susceptibility to misalignment is compared with the performance of the mounting technology, developed at the ILT and demonstrated in “FULAS platform” and the laser for MERLIN. Thereby the remaining effort to achieve space-qualification of the laser concept is estimated.

5.1 Optomechanical components for spaceborne lasers at ILT

Especially spaceborne laser systems require compact, robust and outgassing free key components in order to achieve maintenance free or low-maintenance operation over several years in rough environment. The soldering technique that has been developed for the mounting of diode laser bars as well as solid state laser crystals has been transferred to different laser optical key components. A selection of them is shown in Figure 9 and described in [20] which are mirror and lens mounts as well as Pockels cell packages and Faraday isolators. All of them are complete free from organic material and have been environmentally tested. All of these components were designed to meet the strong requirements for spaceborne laser systems. Especially the mirror mounts meet the extremely high stability requirements against tilting, being $< 10 \mu\text{rad}$, during the whole operational and after the non-operational temperature range and non-operational random vibration spectra.

For the FULAS (Future Laser System) project (see [21]) a complete laser is integrated based on these components. This laser comprises a single-longitudinal mode oscillator and one InnoSlab amplifier stage and successfully completed a multi-week operational ($+10 \text{ }^\circ\text{C}$ to $+30 \text{ }^\circ\text{C}$) and non-operational ($-30 \text{ }^\circ\text{C}$ to $+50 \text{ }^\circ\text{C}$) test in a thermal vacuum chamber at Airbus Defence & Space.

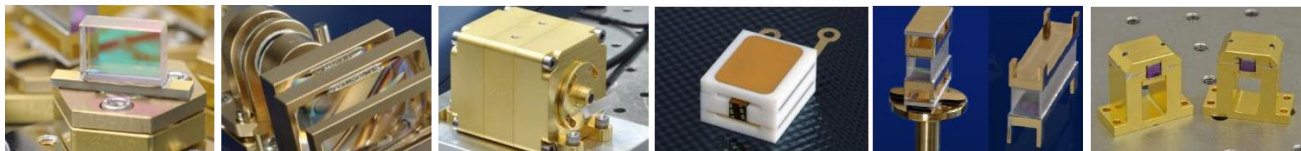


Figure 9. Examples of optomechanical components developed for spaceborne lasers. From left: pick & align mirror mount, reflow-soldered pump optics, Faraday isolator, Pockels cell, NLO crystals and laser crystals.

The diode-pumped Alexandrite lasers presented here comprises, besides the mirrors, a Faraday rotator and a Pockels cell which requirements are fulfilled by the components developed at the ILT for spaceborne operation. Changing the Pockels cell crystal from KD^*P to BBO should be possible since BBO was already used in Q-switched Alexandrite lasers before [16].

5.2 Measurement of the susceptibility to misalignments

Regarding the stability against tilting, the mirrors of the resonator are by far the hardest to fulfill specification. Therefore the susceptibility of the enhanced Alexandrite laser (Figure 7) to misalignments of folding mirror in the resonator is measured. One of the plane folding mirrors is mounted in a piezo-driven mirror mount that has a resolution of $\sim 0.5 \mu\text{rad}$ for a 0.1 V-step.

The mirror is tilted in pitch and yaw separately while the other spatial direction remains unchanged and therefore well aligned. For each tilting step the pulse energy, beam quality and linewidth of the seeded and stabilized laser is measured. The results are shown in Figure 10 for both pitch and yaw.

For a tilting of $\pm 125 \mu\text{rad}$ and $\pm 140 \mu\text{rad}$ in pitch and yaw respectively the pulse energy drops by 10 % while the beam quality in both directions ($M^2 < 1.3$) is still meeting the requirements. Even for a tighter limit of 5 % energy drop, a tilting of $\pm 100 \mu\text{rad}$ both in pitch and yaw is tolerable. The SLM operation is also reliable over a broad tilting ($> \pm 200 \mu\text{rad}$) in both directions.

Beside the tentative mechanical setup and the non-optimized folding for a small footprint, the results indicate that the mirror mounts developed at ILT for spaceborne lasers with tilting $< 10 \mu\text{rad}$ will suffice to set up the resonator.

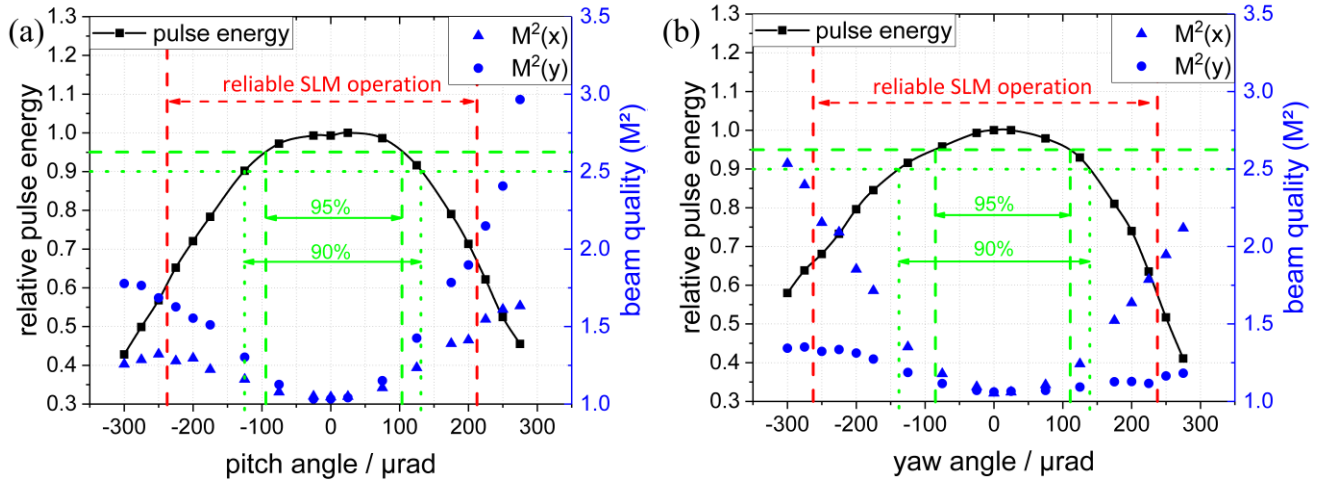


Figure 10. Pulse energy and beam quality of the seeded and stabilized laser for (a) pitch- and (b) yaw-tilting.

5.3 Theoretical analysis

The results for the folding mirror that is tilted is not representative for the other optics. An analytical analysis based on by a 3x3 beam matrix formalism for misaligned optical elements, as described e.g. in [22], allows a conversion of the results to every position within the resonator.

The tolerance analysis of the laser system is conducted analytically, assuming Gaussian beams and a paraxial optical system. Similar attempts have been carried out for simple resonator geometries [23, 24] and for arbitrary resonators [25], but only taking into account the displacement and tilt of the mode. However, the resulting reduction of output power were not described in these papers.

We describe analytically the tilt and displacement of the beam due to misalignment of every optical element within the resonator in Figure 7. Comparing these theoretical dependences with the measured dependence on the misalignment of one mirror, we calculate the dependence of every other optical element.

Theoretical Basics

The tolerance analysis is carried out by a 3x3 matrix formalism as described e.g. in [22]. Here the well-known 2x2 matrix describing the ray transfer through a well-aligned, paraxial optical element or system, given by the matrix elements A, B, C and D, is expanded by two further matrix entries E and F

$$\mathbf{M} = \begin{pmatrix} A & B & E \\ C & D & F \\ 0 & 0 & 1 \end{pmatrix}, \quad (1)$$

where E and F represent the output displacement h_{out} and the tilt θ_{out} of a reference input beam entering the optical element or system described by M on the optical axis collinearly, $h_{in} = \theta_{in} = 0$.

For misaligned optical systems used in a single pass, the analysis is straight forward: Firstly, we define the 3x3 matrix M_i for every single optical element. Here, the matrix entries E_i and F_i are functions of the displacement Δ_i and tilt δ_i of element i compared to a well-aligned optical system. Secondly, we derive the transfer matrix M_S for the overall misaligned system by matrix multiplication of all matrices M_i . Finally, we find the displacement and tilt of the output beam $h_{S,out}$ and tilt $\theta_{S,out}$ as a function of the tilt and displacement of the input beam $h_{S,in}$ and tilt $\theta_{S,in}$ as well as the misalignment of the optical system $\Delta = \{\Delta_i\}$, $\delta = \{\delta_i\}$:

$$\begin{aligned} h_{S,out} &= A_S \cdot h_{S,in} + B_S \cdot \theta_{S,in} + E_S, \\ \theta_{S,out} &= C_S \cdot h_{S,in} + D_S \cdot \theta_{S,in} + F_S. \end{aligned} \quad (2)$$

For misaligned periodic systems or resonators one can define an Eigenproblem for the orientation (h_E, θ_E) of its beam axis according to the optical axis of the well-aligned resonator by means of the roundtrip matrix MR:

$$\begin{pmatrix} h_E \\ \theta_E \\ 1 \end{pmatrix} = \begin{pmatrix} A_R & B_R & E_R \\ C_R & D_R & F_R \\ 0 & 0 & 1 \end{pmatrix} \cdot \begin{pmatrix} h_E \\ \theta_E \\ 1 \end{pmatrix} \quad (3)$$

The Eigenproblem for the q-parameter of a Gaussian beam reproducing itself after a complete resonator roundtrip and the definition of the q-parameter itself are presumed to remain unchanged by the misalignment of the system,

$$q_E = \frac{A_R \cdot q_E + B_R}{C_R \cdot q_E + D_R} \quad , \quad (4)$$

$$q = z + iz_R, \quad z_R = \frac{\pi \cdot w_0^2}{\lambda} \quad , \quad (5)$$

where z_R is the Rayleigh length of the Gaussian beam with a waist radius w_0 . The solution of the Eigenproblem for the misalignment is thereby

$$h_E = \frac{(1 - D_R) \cdot E_R + B_R \cdot F_R}{2 - A_R - D_R} \quad , \quad (6)$$

$$\theta_E = \frac{(1 - A_R) \cdot F_R + C_R \cdot E_R}{2 - A_R - D_R} \quad . \quad (7)$$

Results of the analysis

The analysis verifies the results from the measurement of the susceptibility to misalignment. A tilting of the mirror in the piezo-driven mount of 1 mrad results in a displacement of the laser mode in the laser crystal of 0.28 mm. The 100 μ rad tilting for with the measurement shows a reduction of 5 % of the pulse energy (Figure 10) correlates to a displacement of 28 μ m. This corresponds to a displacement of about 10 % of the pump beam radius and the only slightly reduced overlap of laser mode and pumped crystal volume makes the energy reduction plausible.

The highest susceptibility to misalignment show the mirrors between the two curved mirrors e.g. the output coupler and the mirror mounted on the piezo-actor for stabilization of the cavity length. For those mirrors the displacement of the laser modes is twice as large compared with the mirror in the piezo-driven mount. Therefore the tilting that is acceptable for a pulse energy reduction of 5 % is still ± 50 μ rad and therefore the mirror mounts developed at ILT should be suitable for setting up an Alexandrite laser for spaceborne operation.

6. SUMMARY

In this work the first diode-pumped Alexandrite ring laser in Q-switched single-longitudinal mode operation is presented. A carefully designed and complex ring resonator with several functional components is combined with an innovative pumping scheme with high-power red laser diodes.

The spectral and energetic suitability of the laser was demonstrated in hundreds of operating hours and, with a novel mobile lidar system, by the first measurements in the atmosphere by means of a diode-pumped Alexandrite laser, yielding data from the stratosphere to the mesosphere.

The weak points of the first design were eliminated by an advanced pump concept that lead to enhanced performance and stability. The electro-optical efficiency is the highest archived for all Alexandrite lasers in SLM operation and reasonable for spaceborne operation.

The performance analysis as well as benchmarking with the space-qualified mounting technology point out the TRL and the remaining effort of development of the technology.

7. ACKNOWLEDGMENTS

The work is funded by the German Aerospace Center (DLR) as a representative for the Federal Ministry for Economic Affairs and Energy (BMWi) (FKZ 50RP1605)

REFERENCES

- [1] Kaifler, B., Lübken, F.-J., Höffner, J., Morris, R.J. and Viehl, T. P., "Lidar observations of gravity wave activity in the middle atmosphere over Davis (69° S, 78° E), Antarctica," *J. Geophys. Res. Atmos.*, 120, 4506–4521 (2015).
- [2] Lübken, F.-J., Höffner, J., Viehl, T. P., Becker, E., Latteck, R., Kaifler, B., Murphy, D. and Morris, R.J., "Winter/summer transition in the Antarctic mesopause region," *J. Geophys. Res. Atmos.*, 120(12), 394–12,409 (2015).
- [3] Zhao, J., Chu, X., Chen, C., Lu, X., Fong, W., Yu, Z., Jones, R. M., Roberts, B. R. and Dörnbrack, A., "Lidar observations of stratospheric gravity waves from 2011 to 2015 at McMurdo (77.84°S, 166.69°E), Antarctica: 1. Vertical wavelengths, periods, and frequency and vertical wave number spectra," *J. Geophys. Res. Atmos.*, 122(10), 5041-5062 (2017).
- [4] Lübken, F.-J., Höffner, J., Viehl, T. P., Kaifler, B. and Morris, R. J., "First measurements of thermal tides in the summer mesopause region at Antarctic latitudes," *Geo-phys.Res.Lett.*, 38 (2011).
- [5] Rapp, M., Lübken, F.-J., Müllemann, A., Thomas, G. E. and Jensen, E. J., "Small scale temperature variations in the vicinity of NLC: experimental and model results," *J. Geophys. Res.*, 107 (D19) (2002).
- [6] Höffner, J. and Lübken, F.-J., "Potassium lidar temperatures and densities in the mesopause region at Spitsbergen (78°N)," *J. Geophys. Res.*, 112, D20114 (2007).
- [7] von Zahn, U. and Höffner, J., "Mesopause temperature profiling by potassium lidar," *Geophys. Res. Lett.* 23, 141–144 (1996).
- [8] Lautenbach, J. and Höffner, J., "Scanning iron temperature lidar for mesopause temperature observation," *Appl. Opt.*, 43(23), 4559–4563 (2004).
- [9] Kaifler, B., Büdenbender, C., Mahnke, P., Damm, M., Sauder, D., Kaifler, N. and Rapp, M., "Demonstration of an iron fluorescence lidar operating at 372 nm wavelength using a newly-developed Nd:YAG laser," *Opt. Lett.* 42, 2858-2861 (2017).
- [10] Kawahara, T. D., Nozawa, S., Saito, N., Kawabata, T., Tsuda, T. T. and Wada, S., "Sodium temperature/wind lidar based on laser-diode-pumped Nd:YAG lasers deployed at Tromsø, Norway (69.6°N, 19.2°E)," *Opt. Express* 25, A491-A501 (2017).
- [11] Li, S. X., Yu, A. W., Krainak, M. A., Bai, Y., Konoplev, O., Fahey, M. E. and Numata, K., "Progress on Raman laser for sodium resonance fluorescence lidar," *Proc. SPIE* 10511, 105111H (2018).
- [12] Krainak, M. A., Yu, A. W., Li, S. X., Bai, Y., Numata, K., Chen, J. R., Fahey, M. E., Micalizzi, F., Konoplev, O., Janches, D., Gardner, C. S. and Allan, G. R., "Progress on laser technology for proposed space-based sodium lidar," *Proc. SPIE* 10511, 105111E (2018).
- [13] Walling, J., Peterson, O., Jenssen, H., Morris, R. and O'Dell, E., "Tunable alexandrite lasers," in *IEEE J. Quantum. Electron.*, 16(12), 1302-1315 (1980).
- [14] McKay, J. A. and Wilkerson, T. D., "Diode-pumped alexandrite laser for DIAL and Doppler lidar," *Proc. SPIE* 3127, 124–132 (1997).
- [15] Damzen, M., "Diode-pumped Alexandrite laser: a bright prospect for future space Lidar missions," *Proc. SPIE* 8534B, 81 (2012).
- [16] Thomas, G. M., Minassian, A., Sheng, X. and Damzen, M. J., "Diode-pumped Alexandrite lasers in Q-switched and cavity-dumped Q-switched operation," *Opt. Express* 24(24), 27212–27224 (2016).
- [17] Munk, A., Jungbluth, B., Strotkamp, M., Hoffmann, H.-D., Poprawe, R., Höffner, J. and Lübken, F.-J., "Diode-pumped alexandrite ring laser in single-longitudinal mode operation for atmospheric lidar measurements," *Opt. Express* 26, 14928-14935 (2018).
- [18] Nicklaus, K., Morasch, V., Hoefler, M., Luttmann, J., Vierkötter, M., Ostermeyer, M., Höffner, J., Lemmerz, C. and Hoffmann, D. "Frequency stabilization of Q-switched Nd:YAG oscillators for airborne and spaceborne lidar systems," *Proc. SPIE* 6451, 64511L (2007).

- [19] Wessling, C., Hengesbach, St., Geiger, J., Dolkemeyer, J., Traub, M. and Hoffmann, D., "50 W passively cooled, fiber coupled diode laser at 976 nm for pumping fiber lasers using 100 um fiber bundles," Proc. SPIE 6876, 687614 (2008).
- [20] Löhring, J., Winzen, M., Faidel, H., Miesner, J., Plum, D., Klein, J., Fitzau, O., Giesberts, M., Brandenburg, W., Seidel, A., Schwanen, N., Riesters, D., Hengesbach, S. and Hoffmann, H.-D., "Key optical components for spaceborne lasers," Proc. SPIE 9730, 97300O (2016).
- [21] Hahn, S., Bode, M., Luttmann J. and Hoffmann, H.-D., "FULAS: high energy laser source for future lidar applications," Proc. SPIE 10562, 105620P (2017).
- [22] Siegmann, A. E., [Lasers], University Science Books, 607-613 (1986).
- [23] Hauck, R., Kortz, H. P. and Weber, H., "Misalignment sensitivity of optical resonators," Appl. Opt., 19(4), 598-601 (1980).
- [24] Magni, V., "Resonators for solid-state lasers with large-volume fundamental mode and high alignment stability," Appl. Opt., 25(1), 107-117 (1986).
- [25] Magni, V., "Multielement stable resonators containing a variable lens," J. Opt. Soc. Am. A 4, 1962-1969 (1987).